



**HAL**  
open science

# Amplified Spontaneous Emission from Optical Fibers Containing Anisotropic Morphology CdSe/CdS Quantum Dots Under Continuous Wave Excitation

Palash Kusum Das, Nishant Dhiman, Siva Umapathy, Frédéric Gérôme, Asha  
Bhardwaj

► **To cite this version:**

Palash Kusum Das, Nishant Dhiman, Siva Umapathy, Frédéric Gérôme, Asha Bhardwaj. Amplified Spontaneous Emission from Optical Fibers Containing Anisotropic Morphology CdSe/CdS Quantum Dots Under Continuous Wave Excitation. *Advanced Photonics Research*, 2023, 4 (11), pp.2300167. 10.1002/adpr.202300167 . hal-04227146

**HAL Id: hal-04227146**

**<https://hal.science/hal-04227146v1>**

Submitted on 3 Oct 2023

**HAL** is a multi-disciplinary open access archive for the deposit and dissemination of scientific research documents, whether they are published or not. The documents may come from teaching and research institutions in France or abroad, or from public or private research centers.

L'archive ouverte pluridisciplinaire **HAL**, est destinée au dépôt et à la diffusion de documents scientifiques de niveau recherche, publiés ou non, émanant des établissements d'enseignement et de recherche français ou étrangers, des laboratoires publics ou privés.



# Amplified Spontaneous Emission from Optical Fibers Containing Anisotropic Morphology CdSe/CdS Quantum Dots Under Continuous Wave Excitation

Palash Kusum Das, Nishant Dhiman, Siva Umapathy, Frédéric Gérôme, and Asha Bhardwaj\*

Fiber laser field is typically dominated by rare earth ions as gain material in the core of a silica optical waveguide. Due to their specific emission wavelengths, rare-earth-doped fiber lasers are available only at few predefined wavelengths. However, quantum dots (QDs) are materials which show tunable emission with change in size and composition. Due to such tunability, QDs seem to be promising candidates for obtaining fiber lasers at a spectrum of wavelengths which is not possible using rare earth ions. To replace rare earth ions with QDs, it is of paramount importance that QDs show signatures of optical gain. Herein, the synthesis of asymmetric pod-shaped CdSe/CdS QDs is reported, which demonstrate efficient gain on pumping. The intrinsic gain properties of the QDs are evaluated through transient absorption (TA) spectroscopy. Later, the exquisite QDs are used to fabricate specialty fibers from which amplified spontaneous emission (ASE) is obtained using continuous wave laser pump at room temperature. Finally, emission signal stability is checked by studying photobleaching and controlling the concentration of the QDs.

Yb<sup>3+</sup> rare-earth ion-doped silicate glass active zones in the fiber laser sources operate at predetermined wavelengths that correspond to their respective  $4f-4f$  transitions.<sup>[2-12]</sup> Their definite output wavelengths limit the use of fiber lasers in a wide range of applications.

Quantum dots (QDs) on the other hand, hold unique size, shape, and composition-dependent tunability due to quantum confinement of charge carriers on all three spatial dimensions resulting in discrete band structure thus, facilitating engineering their emission wavelengths and also achieving amplification. Their application<sup>[13-19]</sup> arena increases due to their simpler, low-cost chemical processability and high quantum yields (QYs).

In the matter of gain medium, CdSe nanocrystals with epitaxially grown CdS (CdSe/CdS QDs) have been proven to be excellent candidates for obtaining light amplification and lasing due to their small conduction band offsets<sup>[20-25]</sup> and dependence of wavefunction overlap on morphology and thickness of CdS shell.<sup>[26]</sup> It is also observed that asymmetrically strained structures create large light-heavy hole splitting, lowering the band edge degeneracy and thus dramatically reducing the lasing threshold.<sup>[27-29]</sup> Synthesis and application of heterostructures with complex anisotropic shapes (such as dot-in-rods, rod-in-rods, tetrapods, and octapods) are still in its infancy with regard to the most recent QD lasing technology.<sup>[30-34]</sup>

Keeping in mind the tunable nature of CdSe/CdS QDs with size and gain enhancement for anisotropic morphology, these QDs would be an excellent choice for the replacement of traditional rare-earth ions for realizing fiber lasers at unconventional wavelengths. In recent years, optical properties of QD-doped optical fibers have been extensively studied for their potential applications in fiber-based amplifiers, lasers, and sensors. For instance, Hreibi et al. reported the fabrication and characterization of PbSe QDs doped liquid-core fibers.<sup>[35]</sup> Cheng et al. reported a PbSe QD-doped fiber laser (QDFL) with a ring resonator using colloidal PbSe QDs as gain media.<sup>[36]</sup> Lei Zhang developed a theoretical model of PbSe-doped fibers,<sup>[37,38]</sup> and also investigated the optical properties of PbSe/CdSe QDs-doped fibers.<sup>[39]</sup> Bahrapour et al. investigated PbSe-doped fiber in a single-mode condition.<sup>[40]</sup> Also, numerous works that have been


## 1. Introduction

For the past two decades, fiber lasers have dominated the commercial laser market due to their versatility, output power quality, and flexibility.<sup>[1]</sup> The trivalent Er<sup>3+</sup>, Tm<sup>3+</sup>, Nd<sup>3+</sup>, and

P. K. Das, S. Umapathy, A. Bhardwaj  
Instrumentation and Applied Physics  
Indian Institute of Science  
Bengaluru 560012, India  
E-mail: asha@iisc.ac.in

N. Dhiman, S. Umapathy  
Inorganic and Physical Chemistry  
Indian Institute of Science  
Bengaluru 560012, India

F. Gérôme  
XLIM-UMR 7252  
University of Limoges/CNRS  
123 ave Albert Thomas, 87060 Limoges, CEDEX, France

 The ORCID identification number(s) for the author(s) of this article can be found under <https://doi.org/10.1002/adpr.202300167>.

© 2023 The Authors. Advanced Photonics Research published by Wiley-VCH GmbH. This is an open access article under the terms of the Creative Commons Attribution License, which permits use, distribution and reproduction in any medium, provided the original work is properly cited.

DOI: 10.1002/adpr.202300167

reported on QD amplified spontaneous emission (ASE) have been obtained from colloidal QD medium and are obtained in closely packed thin films.<sup>[41–45]</sup> Moreover, most of the demonstrated ASE is pumped by femtosecond (fs)<sup>[20–24,40]</sup> or nanosecond pumping (quasi continuous wave (CW))<sup>[24,46–48]</sup> or using a cryostat setup.<sup>[46–48]</sup> Although there have been reports on ASE, lasing, and investigation of QDs containing optical fibers, however, not many reports are there about ASE from such specialty fibers.<sup>[5,34–39]</sup>

Herewith, we report anisotropic CdSe/CdS core/shell QDs containing optical fibers for fiber laser applications. The development of such fibers has been done in two steps. First, anisotropic (pod shaped) CdSe/CdS QDs have been fabricated and their morphology optimized for obtaining high optical gain. As-fabricated pod-shaped nanocrystals have been investigated in detail using transient absorption (TA) spectroscopy at 370 and 555 nm excitation wavelength. In the second step, these QDs are used as active gain media in optical fibers. Hollow borosilicate capillaries were filled with the anisotropic morphology QDs dispersed in toluene and investigated for their optical characteristics. Further, ASE has been successfully achieved at room temperature (RT) in specialty QD fibers by varying QD concentration in the fiber and CW pump power. In addition, stability of emission from these QD fibers has also been investigated.

## 2. Results and Discussion

As-prepared CdSe and CdSe/CdS core-shell QDs were investigated for their structural characteristics using transmission electron microscopy (TEM) and high-resolution transmission electron microscopy (HRTEM). CdSe QDs were observed to be spherical in shape (Figure S1a, Supporting Information) with average particle size of 3 nm (inset Figure S1a,b, Supporting Information). *d* values calculated from interplanar distances revealed [100], [110], and [002] planes of hexagonal phase of CdSe (JCPDS No. 65–2891). When high concentration of CdS monomers were injected at high temperatures, CdS rapidly deposited over CdSe QDs which acted as seeds for CdSe/CdS core-shell QD formation. After 15 min of reaction, the spherical QDs transformed into a pyramid shape of size  $\approx 7$  nm (Figure S1c,d, Supporting Information), which further evolved to pod-shaped particles with average size of  $\approx 12$  nm (Figure 1a and S1e,f, Supporting Information). The selected area electron diffraction (SAED) pattern of the pod-shaped structure revealed that the CdS shell formed had a hexagonal phase and confirmed the presence of [111], [220], [311], and [422] planes of CdS (Inset Figure 1a). HRTEM images further supported the pod morphology of the QDs (Figure 1b).

Figure 1c depicts the typical absorption and emission spectrum of CdSe and CdSe/CdS QDs. In the absorption spectra,

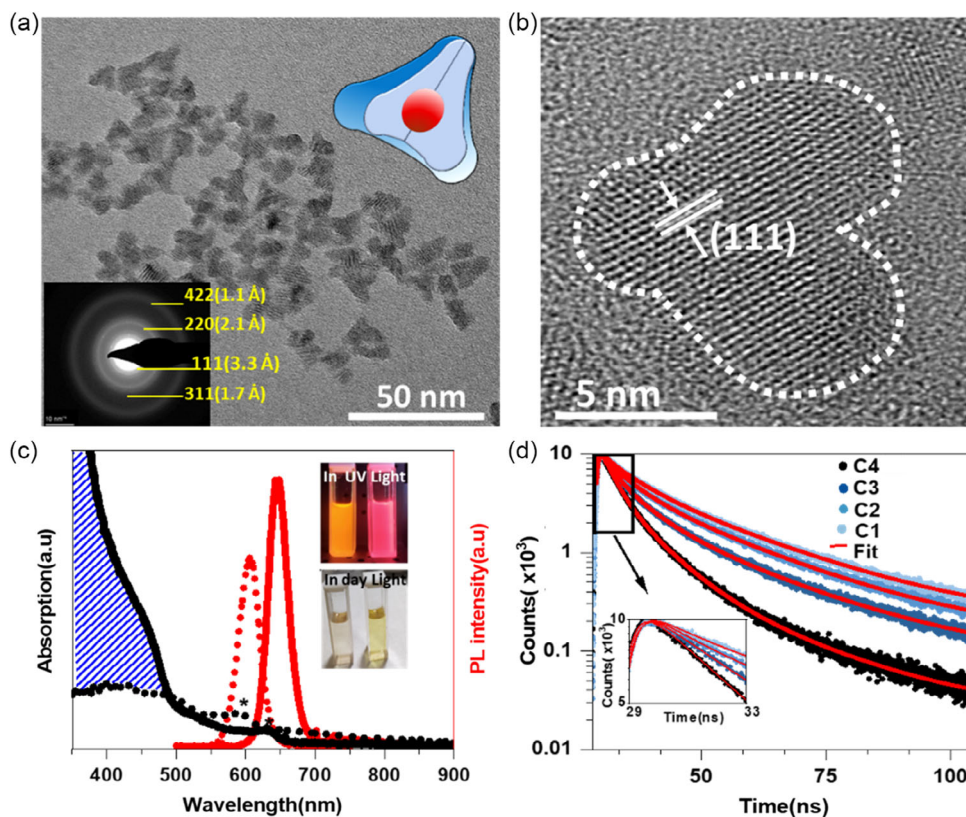


**Figure 1.** TEM images of a) CdSe/CdS core/shell pod-shaped QDs. Inset: SAED pattern of QDs along with schematic of the observed morphology; b) HRTEM image of CdSe/CdS QDs; c) emission spectra (red line) and absorption spectra (black line) of CdSe (dotted line) and CdSe/CdS pod-shaped QDs (continuous line). Inset shows CdSe QDs (on left) and CdSe/CdS QDs (on right) in day light (bottom) and under UV light (top); under UV illumination CdSe QDs emit orange, and CdSe/CdS pod-shaped QDs emit red. d) Fluorescence decay trace for various concentrations of QDs. Inset: Lifetime increase with a decrease in concentration.

excitonic absorption at 590 and 628 nm could be observed for both CdSe and CdSe/CdS core-shell structures. CdSe/CdS QDs showed higher absorption for wavelength <480 nm as compared to CdSe QDs. The CdS shell makes up the majority of volume fraction of the QDs, and thus a strong absorption due to the shell was highly anticipated.<sup>[49,50]</sup> Further, the CdSe QDs emission spectra revealed emission maxima at ≈607 nm which shifted to ≈645 nm for CdSe/CdS core-shell structures. The redshift of the emission maxima can be attributed to the electron delocalization into the shell due to the small offset (0.2 eV) of the conduction band between CdSe and CdS. Low full width at half maximum (FWHM) of emission peaks ≈34 nm for CdSe and ≈36 nm for CdSe/CdS QDs also suggests that the monodispersity of the QDs was maintained after shelling. The effectiveness of shelling is further confirmed by the absence of emission peak from CdS layer (which emits at lower wavelengths<sup>[51]</sup>).

Further, dynamics of radiative exciton recombination are investigated using time-resolved photoluminescence (PL) spectroscopy (Figure 1d). QD solution concentration (16.0, 5.3, 1.8, 0.7 nmol ml<sup>-1</sup>) was altered while the pulse source energy remained constant (4.8 μW at 1 MHz). The number of excitons generated is given by  $\langle N_0 \rangle = j_p \sigma_0$ ,<sup>[52,53]</sup> where  $j_p$  is the pump photon fluence (number of photons per unit area per pulse), and  $\sigma_0$  is the QD absorption cross section. Pump photon fluence ( $j_p$ ) was kept constant and effective exciton generation was controlled by varying the concentration of the QDs. To fit the decay plot, a triexponential curve of the type

$$I(t) = I(0) \sum_{i=0}^3 A_i e^{-t/\tau_i} \quad (1)$$

where  $I(0)$  and  $I(t)$  are the PL intensities at times 0 and  $t$ , respectively.  $\tau_i$  is the excited-state lifetime of each component of PL decay, and  $A_i$  is the relative amplitude of that component. The fastest decay component,  $\tau_1$ , increases from 0.6 ns to 2.0 ns with increasing absorption cross section, attributed to the trap states. Whereas the moderate decay,  $\tau_2$  component, is attributed to non-radiative decay, which increases from 4.41 ns to 6.89 ns with an increase in absorption cross section or decrease in concentration. The slowest decay rate,  $\tau_3$ , has been attributed to single-exciton radiative decay (Table S1, Supporting Information).

To explore the carrier dynamics and optical gain in the pod-shaped CdSe/CdS structures, TA spectroscopy is performed at 370 nm (above band edge) and 555 nm (near-band-edge) excitation wavelengths. The TA spectrum with 370 nm excitation is shown in Figure 2a. A similar TA spectrum is found when excited with 555 nm (Figure 2b). Absorption peaks in the steady-state absorption spectrum (white Figure 2a) match with the first two bleaching bands; the next two transitions, however, were not resolvable (in steady-state absorption spectra) but are clearly evident in the TA spectrum. Bleaching band at 629, 598, 523, and 474 nm has been attributed to the transitions  $1S_e-1Sh_{3/2}$  (1S),  $1S_e-2Sh_{3/2}$  (2S), and  $1P_e-1Ph_{3/2}$  (1P) in CdSe and  $1S_e-1Sh_{3/2}$  of CdS shell.<sup>[54]</sup> Further, bleach spectra at various time intervals between pump and probe have been analyzed (Figure 2c). Since excitation wavelength (370 nm) is

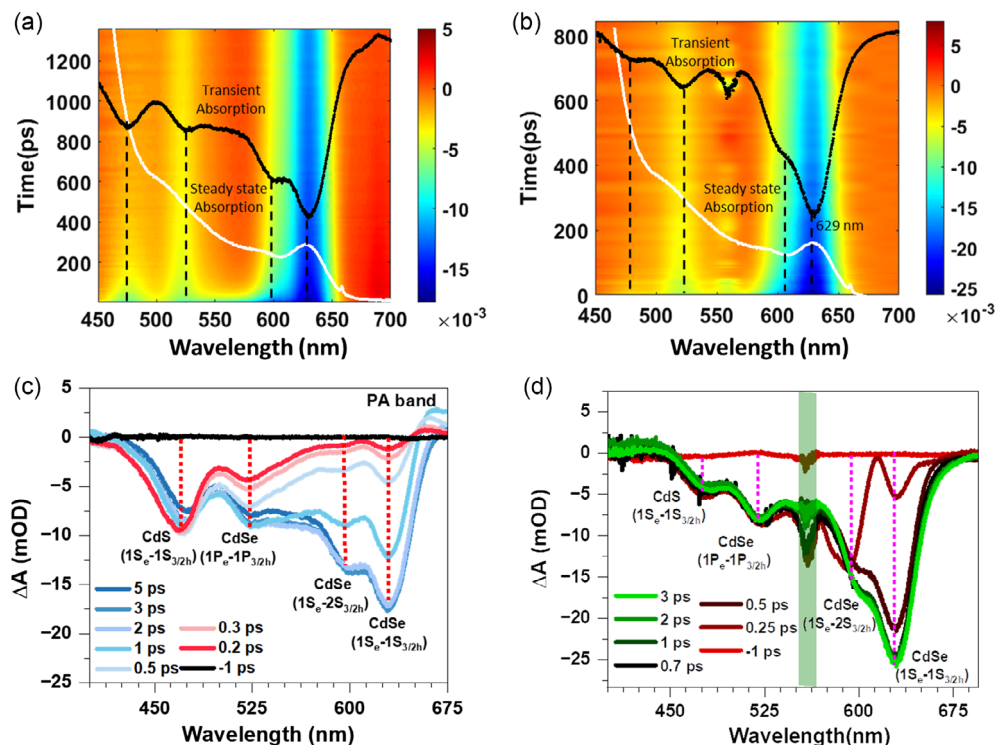


**Figure 2.** Pseudo-color 2D contour plot of time-resolved TA spectra at a) 370 nm and b) 555 nm excitation pump wavelength. Steady-state absorption spectra (white) and bleach spectra (black) are also shown at each wavelength. c, d) Bleach spectra at various time intervals between pump and probe when excited with 370 and 555 nm, respectively.



lesser than CdS absorption edge wavelength, early bleaching at 468 nm is due to the injection of hot charge carriers in CdS (Figure 2c). Bleaching increases as the time delay is changed from 0.1 ps to 0.5 ps. At 0.5 ps, the band reaches its saturation due to complete state filling. Additionally, the bleaching peak at 468 nm shifts to 473 nm with the change in delay time from 0.1 to 0.5 ps. This redshift in the bleaching peak indicates a change in the transition levels caused by biexciton interaction. Further, the 1S and 2S CdSe band bleaching appeared at 0.2 ps, which continued to develop up to 2 ps, whereas the 1P band has been detected from 0.15 ps which saturated in 1 ps. Time delay-dependent bleach spectra prove that hot carriers filled the high-energy excited states CdS band and 1P band. Also, it is evident that core state filling did not occur until the CdS band was completely full. The charge carriers relaxed to the lower-energy state only after completely filling higher-energy states,

following Pauli's exclusion principle. This is the reason for the continuous rise of 1S and 2S bands up to 2 ps, whereas the CdS and 1P were saturated in 0.5 and 1 ps of time, respectively. Additionally, the CdS bleaching band has long lifetimes (Figure 2b), which is primarily due to easily delocalized electrons in these quasi-type-II band-aligned nanostructures. There is also the chance of exciton recombination in the CdS band due to the long life of electrons in this band; however, due to the lack of holes, most of the electrons make their way to the core. With 555 nm excitation, the state filling occurred over the entire QD rather quickly. In 0.5 ps, the CdS and 1P band filled completely and in 0.7 ps the 1S and 2S band reached its saturation (Figure 2d).

In order to quantify the state filling process and exciton formation in pod-shaped QDs, TA kinetics at early time delay, 0–5 ps, has been studied. Figure 3a depicts the transition time

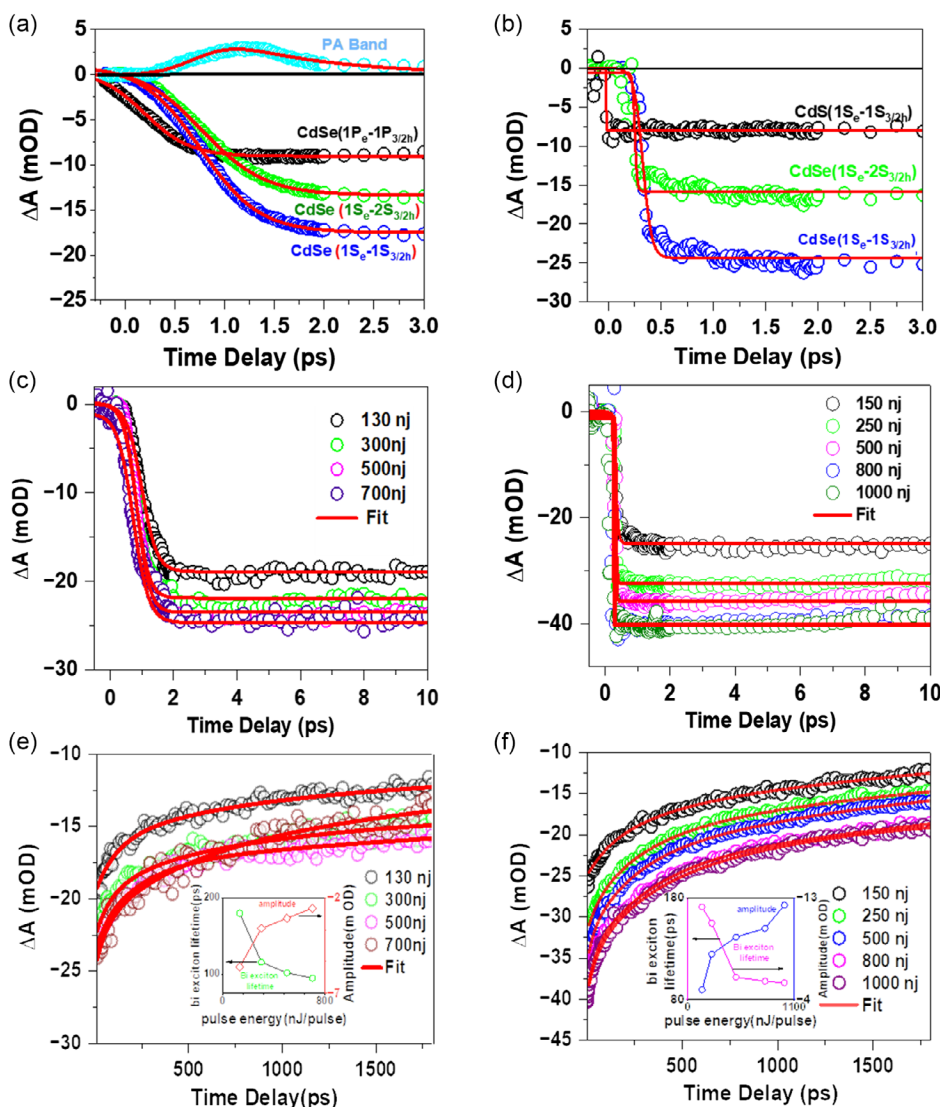


**Figure 3.** Early-time TA signals of different transitions of the CdSe/CdS QDs excited with a) 370 nm and b) 555 nm wavelengths, at fixed pulse energy, 130 nj. c,d) 1S TA signal of the core when pumped with different energy at lower time intervals between pump and probe. Bleaching decay dynamics with pulse energy for e) 370 nm and f) 555 nm. Inset shows the fitted biexciton lifetime and its corresponding amplitude with respect to pulse energy.

or occupancy of electron–hole pairs in the respective bands when pumped with 370 nm excitation wavelength. An exponential curve has been used to fit the TA signals of early time to determine the overall transition and bleach growth time. The rise time for 1P, 2S, and 1S transitions is 0.67, 0.53, and 0.52 ps which is within the limit of Instrument Response Function (IRF) (100 fs). It is also evident that 2S and 1S rise time are same and transitions occurred simultaneously; this is due to the fact that they both share the same  $1S_e$  electron band. The rise time found for the transitions when excited with 555 nm was comparatively shorter (Figure 3b). The rise time for 1P transition is restricted by instrument response function (<0.1 ps) and 2S and 1S transitions have a similar rise time of around 0.2 ps. When 1S transition is compared for both excitations (370 and 555 nm), it is found that though the state filling process in band edge starts at the same instant of time, the rise time is twice as fast with 555 nm excitation (Figure S2b, Supporting Information). As 370 nm excitation creates hot carriers much above the band edge, the slower rise time can be attributed to the relaxation of hot carriers from higher-excited states to the 1S excited state of the exciton.<sup>[55,56]</sup>

Additionally, a photoinduced (PA) band is observed around 660 nm when excited with 370 nm. As shown in Figure S2a, Supporting Information, the PA band has a rise time of 0.5 ps and then decays in same time. It is also found that the build-up time of 1S band is same as decay and build-up time of PA band; this explains that the hot carrier relaxes to the band edge in 0.5 ps. The same PA band is missing with 555 nm excitation, which shows the absence of hot carriers with near-band-edge excitation.

TA kinetics of the 1S state at an early time with variable pulse energy are shown in Figure 3c. With the Boltzmann sigmoidal function fit to the state filling process, it was discovered that regardless of increase in pulse energy the saturation reaches in 0.5 ps. Similarly with 555 nm excitation, the rise time is found to be 0.2 ps, which is consistent with the increase in pulse energy (Figure 3d). Multiexciton generation increases with increase in pulse energy, leading to increase in intrinsic Auger recombination. However, in this case, the saturation of  $\Delta A$  has been identified to be constant up to 10 ps for the highest pulse energy (Figure 3c,d). This saturation in  $\Delta A$  also indicates that there is no electron–hole recombination, and also occupancy of electrons in the  $1S_e$  state and hole occupancy in  $1S_{3/2}$  is in equilibrium. The amount of time for which  $\Delta A$  stays saturated is a direct measure of multiexciton lifetime. The lifetime for  $\Delta A$  saturation increases with the decrease in pulse energy, due to reduction in hot carrier generation and hence reduction in Auger recombination. The corresponding decay kinetics of  $\Delta A$ , from 10 ps to 1800 ps, has been plotted in Figure 3e (370 nm excitation) and Figure 3f (555 nm excitation). Bleaching fits well with a summation of two exponential decays. The shorter lifetime ( $\tau_1$ ) is attributed to biexciton decay, for which the probability to observe stimulated emission is the highest, and the longer one ( $\tau_2 > 1$  ns) is attributed to single-exciton lifetime. The biexciton lifetime has been of major interest since the generation of biexciton is a key requirement to obtain optical gain. The biexciton lifetime and amplitude of the fitting component have been shown with respect to pulse energy in Figure 3e,f's inset. In both the cases, it shows that with an increase in pulse energy the amplitude increases since higher pulse energy would create

more number of biexcitons. However, the lifetime of the biexciton decreases with pulse energy because high energy would create more multiexcitons and thus Auger recombination probability will also increase, leading to a decrease in biexciton lifetime.

In TA spectrum,  $\Delta A$  is obtained, which is absorption after excitation of the sample in ground state  $\Delta A = A_{ex} - A_0$  ( $A_{ex}$  = absorption spectrum when the sample is in an excited state, pump on;  $A_0$  = steady-state absorption, pump off).  $A_0$  is recorded without changing the concentration of the solution so that the same absorption cross section is maintained. Net optical gain, which implies that the photoexcited sample will amplify rather than reduce the probe intensity, is identified by negative values of nonlinear absorbance  $A_{ex} = A_0 + \Delta A$ . Figure 4a,b shows the nonlinear absorbance  $A_{ex}$ , when excited with 370 and 555 nm respectively for 5 ps delay time. As shown, in both cases, the optical gain build-up is significant due to inversion asymmetry break up at anisotropic morphologies. With 370 nm excitation, optical transparency (zero  $\Delta A + A_0$ ) is obtained at 130 nJ pulse<sup>-1</sup> for  $\langle N \rangle = 0.85$ , whereas optical transparency with 555 nm excitation is obtained at 250 nJ for  $\langle N \rangle = 4.00$  (Figure 4a,b). To investigate hot carrier dynamics involved in optical gain of the material in sub-ps timescale, the 1S bleach, PA band, and gain amplitude are compared at two different excitation wavelengths (Figure S3a,b, Supporting Information). It has been observed that for higher energy (370 nm) time, to reach the optical gain regime is slower compared to band-edge energy excitation (555 nm). The absence of optical gain up to 1 ps can be attributed to the PA band, which prevents optical gain by absorbing hot carriers from the band edge. The optical gain starts to build up as the PA band begins to diminish. This is also verified by the optical gain's rising time and the PA band's identical decay period. Since there is no PA band with 555 nm, the optical gain appeared relatively fast (0.3 ps). The evolution of optical gain spectrum with time is demonstrated in Figure 4c,d. When excited with 370 nm, gain window is attained at a wavelength greater than band-edge absorption feature (>628 nm). The gain window extends from 636 to 657 nm at 1.5 ps and from 640 to 647 nm at 100 ps. When excited with 555 nm, the gain window is found to be between 635 to 695 nm at 1.2 ps and 667 to 672 nm at 50 ps. The increase in gain bandwidth is associated with high threshold and low gain lifetime.

Depletion of ground-state carriers to excited states is referred to as “bleaching of the ground state.” Stimulated emission, which is Stokes shifted because of the Coulombic interaction of the biexciton, in relation to the bleach signal and frequently still overlaps with it, follows the QDs' PL spectrum. This is a QD lasing effect (coherent emission). This transmitted signal typically causes increase in negative absorbance peaks in the final spectra because it cannot be separated from the absorption signal. To distinguish between ground-state bleach and stimulated emission, the spectra were deconvolved. In Figure 5,  $\Delta A$  for different pulse energy at a fixed delay time of 5 ps has been deconvoluted with six peaks. The stimulated emission from an ensemble of QDs has been approximated as Gaussian due to Gaussian size distribution of the QDs and its peak position has been approximated from the previously observed nonlinear  $A_{ex}$  spectrum. The stimulated emission band spans the 2S transition since 1S and

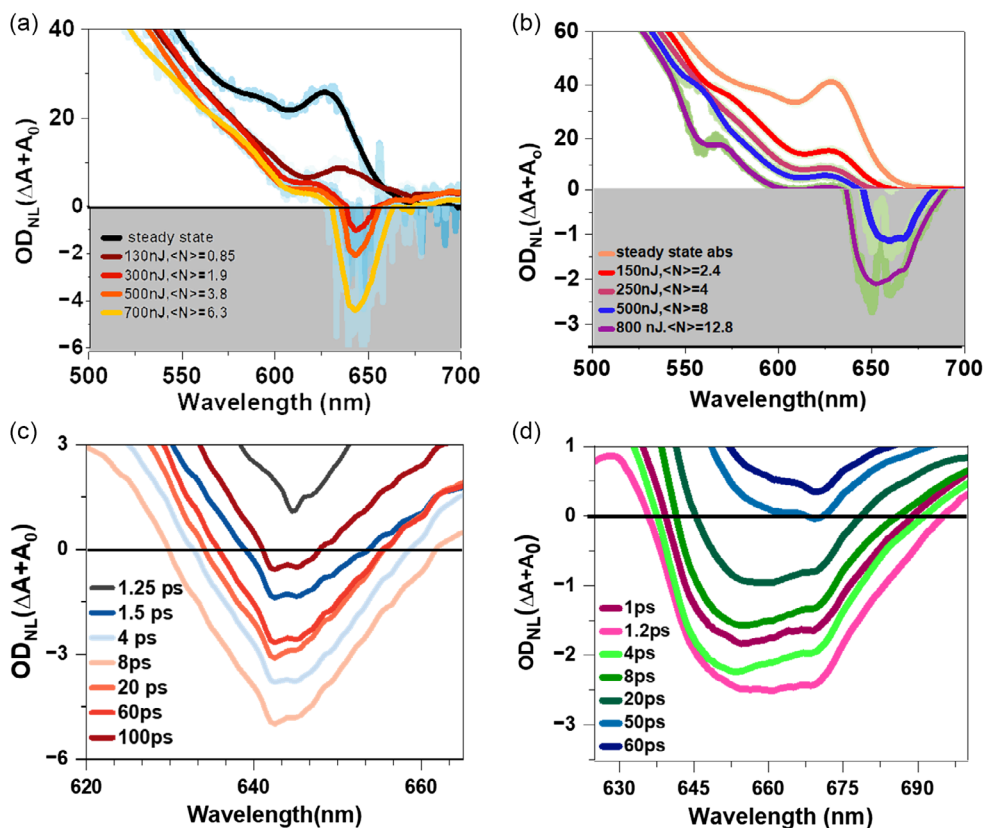


**Figure 4.** Excited-state absorption ( $A_{\text{ex}}$ ) obtained from  $\Delta A + A_0 = A_{\text{ex}}$  at different excitation density (pulse energy),  $\langle N \rangle$ , at 5 ps delay time corresponding to pump wavelength: a) 370 nm and b) 555 nm; Optical gain lifetime corresponding to  $\langle N \rangle = 16$ , using pump wavelength as c) 370 nm, at  $700 \text{ nJ pulse}^{-1}$ , and d) 555 nm, at  $1000 \text{ nJ pulse}^{-1}$ .

2S share a common  $1S_e$  electron occupancy level. It can be seen that a significant signal by stimulated emission overlaps with 1S absorption, which also suggests that net stimulated emission observed from the system will always be redshifted. The area under the stimulated emission peak that did not overlap with an absorption peak representing the intensity of the stimulated emission. The absolute area of this region was found to increase from 0.06 to 0.28 with the increase in pulse energy from 150 to 1000 nJ (covered in black). The spectrum resembles the negative region of  $A_{\text{ex}}$  (Figure 5f), which corresponds to gain or stimulated emission from the QDs.

Owing to the gain in CdSe/CdS QDs, they were entrained in borosilicate hollow capillaries in order to check the effect of waveguide on optical characteristics of QDs. First requisite for confinement of QD emission in the waveguide is higher effective refractive index of the core. A proper investigation of the refractive index ( $n$ ) of QD solution is carried out in order to check the waveguiding properties of the QD-doped fiber. From the refractive index of the curve,<sup>[57]</sup> it can be observed that  $n$  is almost constant ( $n = 1.51$ ) from 450 to 750 nm (Figure S4, Supporting Information), with a negligible variation of 1%. Since 532 nm pump is being used to excite QDs in the core of the fiber, emission is at 650 nm; therefore, it is safe to conclude that  $n$  is constant in the region of interest. Further, refractive index of capillary-clad borosilicate glass at 650 nm is 1.51, ensuring total

internal reflection in the core. The numerical aperture of these fibers filled with different concentrations of QDs has been shown in Table S2, Supporting Information.

The QD-filled fiber was first observed under an optical microscope, to confirm the uniform filling of QD solution inside the fiber. A longitudinal and transverse optical image of the fiber before and after filling with QD solution was taken (Figure 6a–d). To obtain the absorption spectra of the QD-filled fiber, first the fiber was filled with toluene and then a white light source was coupled with a  $20\times$  objective lens; the spectra were collected using optical spectrum analyzer (OSA). Later the same fiber was filled with QD–toluene solution and spectra were collected after coupling with the white light source. For obtaining the PL emission, the same fiber was coupled with 532 nm CW laser and emission was recorded in OSA. Figure S5, Supporting Information, depicts the uniformly filled QD fiber emitting orange when coupled with a 532 nm green laser source.

Both absorption and emission spectra are redshifted in QD-filled fibers as compared to QDs in a cuvette (Figure 6e). The redshift can be attributed to a phenomenon called reabsorption–emission due to overlap between emission and absorption spectrum as observed in Figure 6e, which weakens the signal from smaller QDs. Another reason for such a redshift could be interaction between the borosilicate and QD in toluene interface. Further, emission characteristics of QD-filled fibers were studied by varying



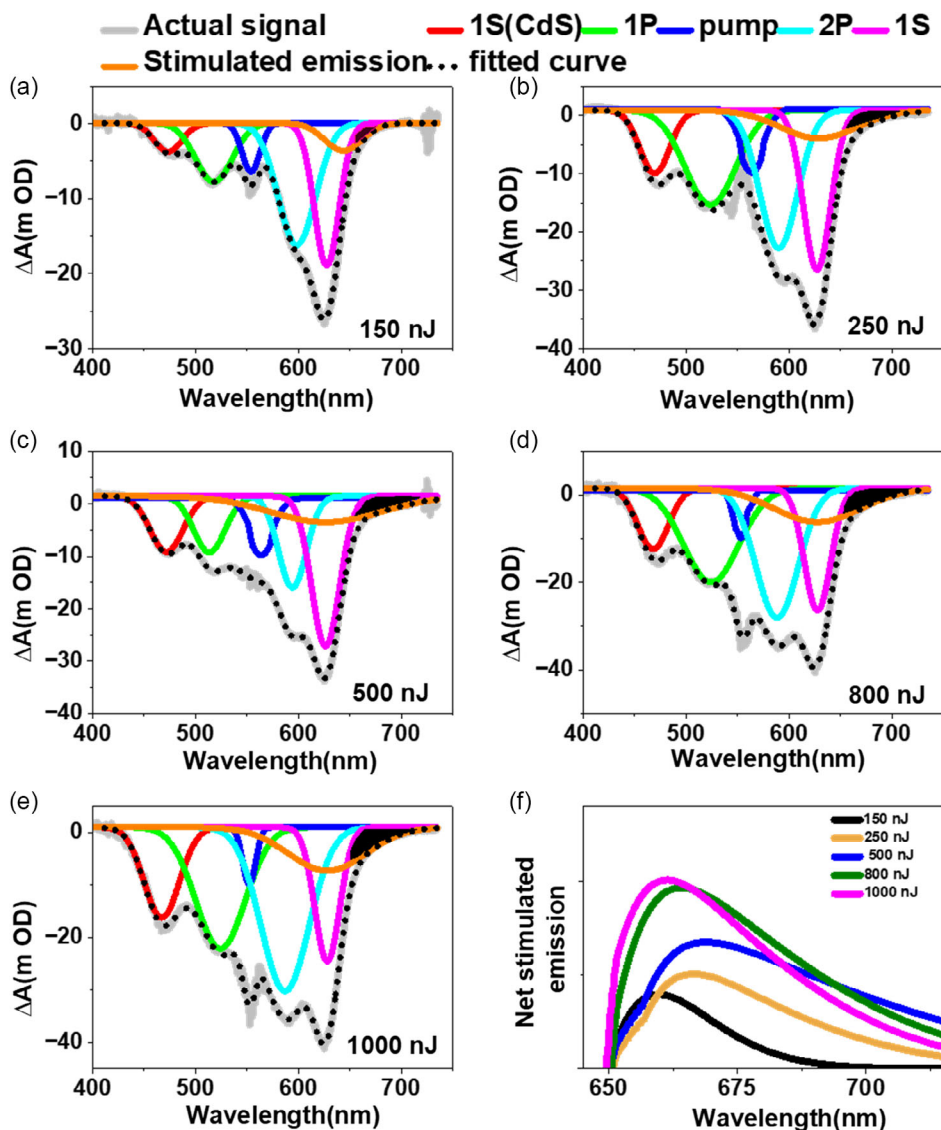


**Figure 5.** Deconvoluted  $\Delta A$  for different pulse energies: a) 150 nJ; b) 250 nJ; c) 500 nJ; d) 800 nJ; e) 1000 nJ. f) Stimulated emission signal extracted at each pulse energy.

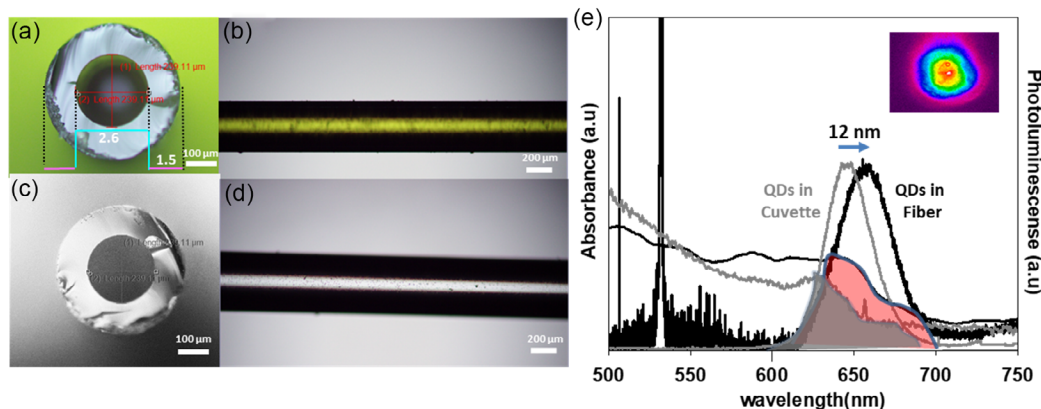


**Figure 6.** a) Vertical and b) horizontal cross section of a hollow capillary. c) Vertical and d) horizontal cross section of a capillary filled with QDs (core diameter = 240  $\mu\text{m}$ , length = 20 cm). e) Absorbance and PL of QD solution in a cuvette (gray) and QD-doped fiber (black). Inset: Near-field image of the core shows the multimode behavior of QD emission in the core.

the fiber length from 35 to 120 cm (60  $\mu\text{m}$  core radius) at 10 mW of pump power. It is observed that the intensity of emission decreases and peak position shifts to a longer wavelength (Inset Figure S4, Supporting Information) with the increase in length of the fiber.

Evolution of emission spectrum by varying the core diameter of QD-filled fibers has also been studied (Figure S7, Supporting Information). Fiber with core diameters of 110, 240, 275, 370, and 535  $\mu\text{m}$  with equal lengths (35 cm) have been filled with the same concentration of QD solution and pumped with 10 mW CW green laser. It can be seen that the intensity of transmitted emission spectra increases initially with increase in core diameter from 110 to 275  $\mu\text{m}$ . With further increase in the core diameter, the emission intensity drops down. Initially on increasing the fiber diameter the pump power will be distributed over a larger area and a greater number of QDs can be excited, leading to an increase in intensity. By further increasing the diameter, the pump power will have more spread due to which it will be totally absorbed on short propagation and the rest of the length will then be a source of loss due to the liquid medium leading to a decrease in emission intensity.

It has been shown that through fs pumping the QDs dispersed in toluene show optical gain for appropriate pump powers (Figure 3d). The emission taken from QD fibers, filled with different concentrations of QD solution is shown in Figure 7a. It is observed that with increase in concentration the

emission maxima redshifts. Further, at QD concentration  $\approx 330 \text{ nmol mL}^{-1}$ , a separate peak shows up. The redshift in emissions can be attributed to the growth of ASE. To further confirm the ASE, a comparison of the emission spectra from QD fiber, QDs in a cuvette, and gain obtained from fs pumping of the QDs are illustrated in Figure 7b. It is clear that the assigned ASE signal overlaps with the gain obtained from fs pumping. Also, it is evident that the emission spectrum from QD fibers is a superposition of two phenomena: spontaneous emission from QDs (645 nm) and ASE (669 nm). This is also illustrated by deconvoluting the emission spectra (Figure 7c) using a Gaussian profile. The peak position of the Gaussian corresponding to Spontaneous emission has been fixed from the PL peak of the QDs in solution (645 nm), whereas the ASE Gaussian peak has been chosen from the gain spectrum that has been obtained from fs pumping. As the concentration is increased from 10 to 330  $\text{nmol mL}^{-1}$ , the packing fraction,  $\xi$ , also increases from 0.01 to 0.43 and thus there is a better chance of observing ASE.<sup>[53,58]</sup> This is directly evident from these data that the contribution from spontaneous emission decreases while that from ASE increases with increase in packing fraction.

In order to investigate ASE further, the high concentration of QDs were exposed to different pump powers. It was anticipated that at higher concentration, due to enhanced QD–QD interaction, emission from a QD will trigger a chain of downfall of excitons to the ground state in which the radiation from one

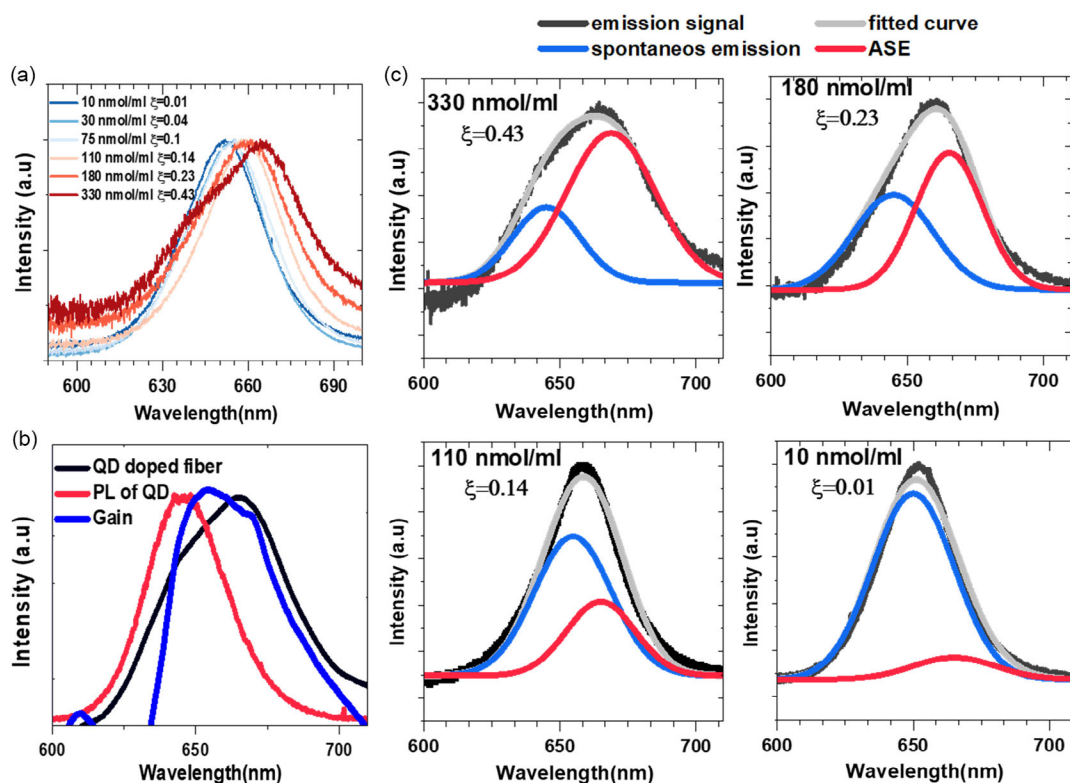


**Figure 7.** a) Variation in emission spectra with concentrations of CdSe/CdS QDs in hollow glass capillaries of diameter (275  $\mu\text{m}$ ) and length (70 cm) excited with fixed pump power (50 mW). b) Comparison of PL spectra of QDs in a cuvette, gain obtained from TA spectrum (pump wavelength 555 nm) and PL of QD-filled fiber with the highest concentration of QD solution at pump power 400 mW. c) Peak fitted for emission spectra obtained from QD-filled fiber with different concentrations, to have a quantitative idea of spontaneous emission and ASE.

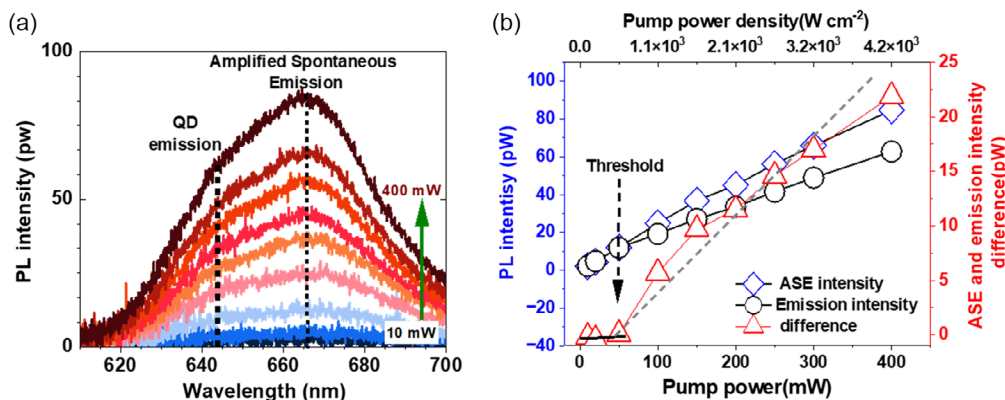


**Figure 8.** a) Development of ASE band at  $\approx 669$  nm is observed as a function of CW pump power. Pump power is varied from 10 to 400 mW. b) The ASE band is seen to grow linearly. A definite threshold of 50 mW ( $520 \text{ W cm}^{-2}$ ) is shown when the strong spontaneous PL that is present in the ASE spectrum's background is subtracted.

QD stimulates another in succession, resulting in stimulated emission. Also, high pump power would ensure minimal reabsorption and QDs are excited through pump power only. Emission from  $330 \text{ nmol mL}^{-1}$  has been obtained by exposing the QD fibers to pump powers varying from 10 to 400 mW. The emission spectrum taken for the fiber filled with  $330 \text{ nmol mL}^{-1}$  concentration of QDs is shown in Figure 8a. The spontaneous emission peak from the QDs and ASE peak has been identified. It is clear that with the increase in pump power, the ASE peak gets intensified. The peak power corresponding to these two phenomena and their power difference is shown in Figure 8b. Following the subtraction of the background resulting from the "saturated" spontaneous emission, this new band shows a well-defined threshold ( $\approx 520 \text{ W cm}^{-2}$ ) and a clear linear growth; both of these observations are signatures of the ASE.

To obtain ASE, high powers (0.4 kW) have been used which may lead to degradation of the QDs through photobleaching. To understand photobleaching and get an estimate of maximum power which these QDs can sustain in fiber without degradation, a highly concentrated ( $330 \text{ nmol mL}^{-1}$ ) and a highly diluted ( $5 \text{ nmol mL}^{-1}$ ) QD solution drop cast on a glass slide were kept under a confocal microscope and exposed to a green 532 nm CW

laser with excitation power of 200 mW. The beam has been focused with  $60\times$  scope (spot size =  $0.6 \mu\text{m}$ ), making the intensity to be  $100 \text{ kW cm}^{-2}$ . The intensity was collected with a charge coupled device (CCD) camera with time (Figure S8, Supporting Information). Later the image's overall intensity was calculated over an area, the intensity drops down with time and the intensity versus time curve was fit with a decay curve (Figure 9a). With diluted solution, time taken ( $t$ ) for intensity to reach  $e^{-1}$  from initial intensity was 13 s, whereas, when a concentrated solution was irradiated under the same condition,  $t$  was 138 s. This suggests that with increase in the number of QDs, the heat produced by the laser gets more distributed and hence the occurrence of photobleaching gets minimized.

To test the stability of QD fiber under high power, a 70 cm QD fiber with a uniform core diameter ( $110 \mu\text{m}$ ) was constantly irradiated with 400 mW laser for 30 min. Emission spectra recorded after every 5 min shows that maximum intensity appeared at time = 0 s (Figure 9b). On further exposure to such high pump power, intensity dropped by 25% in 5 min and then the emission intensity was constant. This indicates that QDs present at the beginning of the fiber receive most of the power which are photobleached faster, whereas rest of the QDs present over the length of the fiber remains unaffected and hence

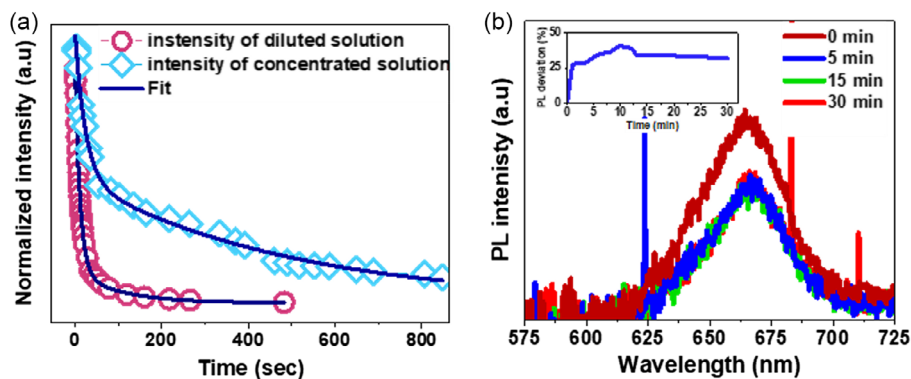


**Figure 9.** a) Variation of normalized PL intensity with time for diluted and concentrated CdSe/CdS QDs. b) Emission spectrum of QD-filled fiber with time, under 400 mW power exposure. Inset shows PL peak intensity variation with time. Emission intensity stays constant for 5–30 min of exposure.

emission remains constant after 5 min. Thanks to large surface-to-volume ratio of the fiber which leads to natural cooling, the emission signal from the fiber remains unaffected with time.

### 3. Conclusion

In conclusion, we have synthesized asymmetric-shaped pod-shaped CdSe/CdS QDs which show efficient optical gain through fs pumping. The same QDs were used to fabricate the specialty fiber. The emission properties of the QDs were characterized. Later, ASE build up in this fiber has been shown with increase in concentration of the QDs, that is, an increase in packing fraction under CW excitation. Also, ASE has been demonstrated with increase in pump power with clear indication of the threshold power  $520 \text{ W cm}^{-2}$ . These results suggest the feasibility that an actual fiber laser with tunable emission is possible with implementation of proper cavity.

### 4. Experimental Section

**Synthesis of CdSe/CdS Quantum Dots:** The CdSe/CdS core-shell QDs were fabricated by a colloidal synthesis technique. 0.2 mmol CdO, 8 mL octadecene (ODE), 8.2 mL of oleylamine (OAm), and 0.3 mL oleic acid (OA) were placed in a 250 mL 3-neck flask and degassed for 10 min. The solution was further heated to 270 °C under argon-gas flow. At this temperature, 2 mmol TriOctylphosphine (TOP)-Se in 2 mL of ODE suspension was quickly injected into the flask, and the reaction was allowed to proceed for 5 min. Finally, the reaction mixture was cooled to room temperature, and an extraction procedure by centrifugation using ethanol for 10 min was performed to purify the QDs from side products and unreacted precursors. For shelling, the QDs were redispersed in 4 mL of ODE in a three-neck flask and degassed for 10 min and the temperature was set to 200 °C. At this temperature, 1 mmol of sulfur dissolved in TOP and ODE was injected into the three-neck flask. After 60 min, 2 mmol of previously prepared Cd-oleate dissolved in ODE was injected. The temperature was further maintained for 60 min and allowed to cool down to room temperature before the extraction procedure. After purification, the QDs were dispersed in toluene and used for further characterization.

**Fabrication of CdSe/CdS-Filled Optical Fiber:** The QDs dispersed in toluene at different concentrations were filled in inhouse-fabricated borosilicate capillaries with different core diameters ranging from 110 to 537  $\mu\text{m}$ . Filling of the fiber was done by submerging one end of the hollow capillary in QD solution and by pressure pulling the QD solution from the other end.

**Characterization:** UV-vis absorption spectra was collected on S 600 Analytik-jena. PL spectra of QDs were recorded using ocean optics USB200. TEM and HRTEM images were obtained on TEM-TITAN Themis. Lifetime was calculated using Horiba Jobin Yvon Fluorocube -01-NL Fluorescence Lifetime System. For characterization of the QD-filled fiber CW-532 nm (GEM532, Laser Quantum), OSA (AQ6374, Yokogawa) and supercontinuum source (LEUKOS) were used.

**Transient Absorption Spectroscopy:** A Ti: sapphire regenerative amplifier (Spitfire, Spectra-Physics) with an output of about  $2 \text{ mJ pulse}^{-1}$ , pulse width 100 fs, and a center at 790 nm was used to amplify seed pulses of 100 fs that were produced by a Ti: sapphire oscillator (Tsumani, Spectra Physics) at a repetition rate of 1 KHz. A beam splitter was used to divide the enhanced 1 mJ  $\text{energy}^{-1}$  pulses into two equal parts (95:5). TOPAS-C (Spectra-Physics) was pumped with 95% of the available energy to create an actinic pump with a 370 nm center. To create a broadband super-continuum white light (380–720 nm) probe, the remaining 5% of the light was focused on a 3 mm CaF<sub>2</sub> crystal. At Magic angle (54.70°), the pump and probe beams were maintained. Both the beam were spatially overlapped on the moving 1 mm sample cuvette to avoid photodegradation of the sample. A transmitted white light probe and reference

beam were selected to enter into the spectrograph (Triax 550, Horiba) and dispersed by 150 mm grooves mm grating<sup>-1</sup>.

### Supporting Information

Supporting Information is available from the Wiley Online Library or from the author.

### Acknowledgements

The authors acknowledge the MNCF facility at CeNSE, Indian Institute of Science, Bangalore. The authors would like to thank MEITY, MHRD for financial assistance.

### Conflict of Interest

The authors declare no conflict of interest.

### Data Availability Statement

The data that support the findings of this study are available from the corresponding author upon reasonable request.

### Keywords

amplified stimulated emission, fiber lasers, optical gain, quantum dots

Received: June 5, 2023

Revised: July 18, 2023

Published online:

- [1] D. J. Richardson, J. Nilsson, W. A. Clarkson, *J. Opt. Soc. Am. B* **2010**, 27, B63.
- [2] B. Bouzid, in *2013 Saudi Inter. Electronics, Communications and Photonics Conf. (SIEPC 2013)*, Riyadh, Saudi Arabia 27–30 April **2013**, pp. 80–84.
- [3] <https://www.ipgphotonics.com/en/products/lasers/high-power-cw-fiber-lasers>, for high power fiber laser product offerings from IPG Photonics, Oxford, MA, USA.
- [4] P. D. Dragic, M. Cavillon, J. Ballato, *Appl. Phys. Rev.* **2018**, 5, 041301.
- [5] A. Bhardwaj, A. Hreibi, W. W. Yu, C. Liu, J. Heo, J.-L. Auguste, J.-M. Blondy, F. G er me, *2012 14th Inter. Conf. on Transparent Optical Networks (ICTON)*, Coventry, UK **2012**, paper no. We.C1.2.
- [6] a) M. J. F. Digonnet, in *Rare-Earth-Doped Fiber Lasers and Amplifiers*, 2nd ed., CRC Press, Boca Raton **2001**; b) E. Desurvire, *Erbium-Doped Fiber Amplifiers: Principles and Applications*, John Wiley & Sons, New York **1994**, p. 112.
- [7] M. G. Brik, T. Ishii, A. M. Tkachuk, I. Tanaka, *Mater. Trans.* **2004**, 45, 2026.
- [8] G. H. Dieke, H. M. Crosswhite, *Appl. Opt.* **1963**, 2, 675.
- [9] R. Reisfeld, A. Patra, G. Panczer, M. Gaft, *Opt. Mater.* **1999**, 13, 81.
- [10] M. Hemenway, W. Urbaneck, D. Dawson, Z. Chen, L. Bao, M. Kanskar, M. DeVito, D. Kliner, R. Martinsen, *Proc. SPIE* **2017**, 10086, 1008605.
- [11] Y. Kasai, S. Sakamoto, Y. Takahashi, K. Katagiri, A. Sakamoto, *Tech. Rev.* **2016**, 42, 6.
- [12] J. Biesenbach, in *2012 IEEE Photonics Society Summer Topical Meeting Series*, IEEE, Piscataway, NJ **2012**, paper no. MA4.3.
- [13] G. Dong, H. Wang, G. Chen, Q. Pan, J. Qiu, *Front. Mater.* **2015**, 2, 13.



- [14] J. Zhao, J. A. Bardecker, A. M. Munro, M. S. Liu, Y. Niu, I.-K. Ding, J. Luo, B. Chen, A. K.-Y. Jen, D. S. Ginger, *Nano Lett.* **2006**, *6*, 463.
- [15] W. Cao, C. Xiang, Y. Yang, Q. Chen, L. Chen, X. Yan, L. Qian, *Nat. Commun.* **2018**, *9*, 2608.
- [16] H. Zhang, S. Chen, X. W. Sun, *ACS Nano* **2018**, *12*, 697.
- [17] R. Din, Y. Chen, Q. Wang, Z. Wu, X. Zhang, B. Li, L. Lin, *J. Pharm. Anal.* **2022**, *12*, 355.
- [18] L. Yun, Y. Qiu, C. Yang, J. Xing, K. Yu, X. Xu, W. Wei, *Photon. Res.* **2018**, *6*, 1028.
- [19] A. M. Wagner, J. M. Knipe, G. Orive, N. A. Peppas, *Acta Biomater.* **2019**, *94*, 44.
- [20] M. Zavelani-Rossi, M. G. Lupo, R. Krahné, L. Manna, G. Lanzani, *Nanoscale* **2010**, *2*, 931.
- [21] M. Zavelani-Rossi, R. Krahné, G. Della Valle, S. Longhi, I. R. Franchini, S. Girardo, F. Scotognella, D. Pisignano, L. Manna, G. Lanzani, F. Tassone, *Laser Photon. Rev.* **2012**, *6*, 678.
- [22] I. Moreels, G. Rainò, R. Gomes, Z. Hens, T. Stöferle, R. F. Mahrt, *Adv. Mater.* **2012**, *24*, OP231.
- [23] F. Di Stasio, J. Q. Grim, V. Lesnyak, P. Rastogi, L. Manna, I. Moreels, R. Krahné, *Small* **2015**, *11*, 1328.
- [24] V. Pinchetti, F. Meinardi, A. Camellini, G. Sirigu, S. Christodoulou, W. K. Bae, F. De Donato, L. Manna, M. Zavelani-Rossi, I. Moreels, V. I. Klimov, S. Brovelli, *ACS Nano* **2016**, *10*, 6877.
- [25] L. Wang, K. Nonaka, T. Okuhata, T. Katayama, N. Tamai, *J. Phys. Chem. C* **2018**, *122*, 12038.
- [26] W. Lin, Y. Niu, R. Meng, L. Huang, H. Cao, Z. Zhang, H. Qin, X. Peng, *Nano Res.* **2016**, *9*, 260.
- [27] F. Fan, O. Voznyy, R. P. Sabatini, K. T. Bicanic, M. M. Adachi, J. R. McBride, K. R. Reid, Y. S. Park, X. Li, A. Jain, R. Quintero-Bermudez, *Nature* **2017**, *544*, 75.
- [28] Y. S. Park, J. Lim, V. I. Klimov, *Nat. Mater.* **2019**, *18*, 249.
- [29] J. Lim, Y.-S. Park, V. I. Klimov, *Nat. Mater.* **2018**, *17*, 42.
- [30] C. D. Sonnichsen, T. Kipp, X. Tang, P. Kambhampati, *ACS Photonics* **2019**, *6*, 382.
- [31] A. Castelli, B. Dhanabalan, A. Polovitsyn, V. Caligiuri, F. Di Stasio, A. Scarpellini, R. Brescia, M. Palei, B. Martín-García, M. Prato, L. Manna, *Adv. Opt. Mater.* **2020**, *8*, 1901463.
- [32] R. Brescia, K. Miszta, D. Dorfs, L. Manna, G. Bertoni, *J. Phys. Chem. C* **2011**, *115*, 20128.
- [33] S. Deka, K. Miszta, D. Dorfs, A. Genovese, G. Bertoni, L. Manna, *Nano Lett.* **2010**, *10*, 3770.
- [34] X. Wang, *J. Phys. Chem. C* **2019**, *123*, 19238.
- [35] A. Hreibi, *Opt. Lett.* **2011**, *36*, 1695.
- [36] C. Cheng, J. Bo, J. Yan, X. Cheng, *IEEE Photon. Technol. Lett.* **2013**, *25*, 572.
- [37] L. Zhang, Y. Zhang, H. Wu, T. Zhang, P. Gu, H. Chu, T. Cui, Y. Wang, H. Zhang, J. Zhao, W. W. Yu, *J. Nanopart. Res.* **2013**, *15*, 2000.
- [38] L. Zhang, B. Zhang, S. Li, Q. Zhu, Y. Zheng, *Opt. Commun.* **2016**, *369*, 171.
- [39] L. Zhang, L. Zhao, Y. Zheng, *Opt. Mater. Express* **2018**, *8*, 3551.
- [40] A. R. Bahrapour, H. Rooholamini, L. Rahimi, A. A. Askari, *Opt. Commun.* **2009**, *282*, 4449.
- [41] S. Bisschop, P. Geiregat, T. Aubert, Z. Hens, *ACS Nano* **2018**, *12*, 9011.
- [42] B. Guzelurk, Y. Kelestemur, K. Gungor, A. Yeltik, M. Z. Akgul, Y. Wang, R. Chen, C. Dang, H. Sun, H. V. Demir, *Adv. Mater.* **2015**, *27*, 2741.
- [43] G. L. Whitworth, M. Dalmases, N. Taghipour, G. Konstantatos, *Nat. Photon.* **2021**, *15*, 738.
- [44] P. Chhantyal, S. Naskar, T. Birr, T. Fischer, F. Lübkemann, B. N. Chichkov, D. Dorfs, N. C. Bigall, C. Reinhardt, *Sci. Rep.* **2018**, *8*, 3962.
- [45] J. Cassidy, B. T. Diroll, N. Mondal, D. B. Berksky, K. Zhao, D. Harankahage, D. Porotnikov, R. Gately, D. Khon, A. Proppe, M. G. Bawendi, *ACS Nano* **2022**, *16*, 3017.
- [46] X. Wang, J. Yu, R. Chen, *Sci. Rep.* **2018**, *8*, 17323.
- [47] Y. Wang, K. S. Leck, V. D. Ta, R. Chen, V. Nalla, Y. Gao, T. He, H. V. Demir, H. Sun, *Adv. Mater.* **2015**, *27*, 169.
- [48] P. Brenner, O. Bar-On, M. Jakoby, I. Allegro, B. S. Richards, U. W. Paetzold, I. A. Howard, J. Scheuer, U. Lemmer, *Nat. Commun.* **2019**, *10*, 988.
- [49] L. Carbone, C. Nobile, M. De Giorgi, F. D. Sala, G. Morello, P. Pompa, M. Hytch, E. Snoeck, A. Fiore, I. R. Franchini, M. Nadasan, *Nano Lett.* **2007**, *7*, 2942.
- [50] J. X. Xu, Y. Yuan, M. Liu, S. Zou, O. Chen, D. Zhang, *Anal. Chem.* **2020**, *92*, 5346.
- [51] V. T. Lien, C. V. Ha, N. N. Dat, *J. Phys.: Conf. Ser.* **2009**, *187*, 012028.
- [52] V. I. Klimov, A. A. Mikhailovsky, S. Xu, A. Malko, J. A. Hollingsworth, A. C. Leatherdale, H. J. Eisler, M. G. Bawendi, *Science* **2000**, *290*, 314.
- [53] V. I. Klimov, A. A. Mikhailovsky, D. W. McBranch, C. A. Leatherdale, M. G. Bawendi, *Am. Assoc. Adv. Sci.* **2000**, *287*, 1011.
- [54] P. Maity, T. Debnath, H. N. Ghosh, *J. Phys. Chem. C* **2015**, *119*, 26202.
- [55] J. Huang, Z. Huang, Y. Yang, H. Zhu, T. Lian, *J. Am. Chem. Soc.* **2010**, *132*, 4858.
- [56] H. Zhu, N. Song, T. Lian, *J. Am. Chem. Soc.* **2010**, *132*, 15038.
- [57] N. A. Hamizi, *Int. J. Electrochem. Sci.* **2012**, *7*, 8458.
- [58] R. D. Schaller, M. A. Petruska, V. I. Klimov, *J. Phys. Chem. B* **2003**, *107*, 13765.